Revisiting the SDI and ECCS methods for in-plane shear flexibility of metal roof deck diaphragms using 3D non-linear finite element analysis

F. Bakhti & R. Tremblay
Ecole Polytechnique de Montreal, Canada

C.A. Rogers
McGill University, Canada

15 WCEE
LISBOA 2012

ABSTRACT:
Corrugated metal roof deck panels are commonly used to form horizontal diaphragms which carry lateral loads in low-rise steel buildings. These thin steel panels are fastened to each other and to the supporting steel framework in order to develop diaphragm action in the roof of a building. This paper describes a numerical simulation with regards to the shear behaviour of the diaphragm. The results of a 3D non-linear finite element analyses are presented, for which representative diaphragm configurations have been subjected to in-plane loading. The analyses indicate that the total in-plane flexibility of the diaphragm is the sum of the sheet flexibility including warping deformations, the shear flexibility of the connections, and a correction factor that accounts for the interaction between the panels and their connections. Comparison with the current Steel Deck Institute (SDI) and European Convention for Constructional Steelwork (ECCS) design methods for steel deck diaphragms and experimental data is also presented.

Keywords: Steel deck, Diaphragm, Shear panel, Sheet warping, Fasteners

1. INTRODUCTION

Extensive testing and several analytical investigations have been carried out in North America (Nilson, 1960; Luttrell and Ellifritt, 1970; Tremblay et al., 2008) and Europe (Davies, 2006) to determine the in-plane shear stiffness, G', properties of metal roof deck diaphragms. Inconsistencies with recent field test programs of low-rise steel buildings under ambient and forced vibration (Proulx et al., 2012; Lamarche et al., 2009) as well as laboratory experiments of representative steel diaphragms (Tremblay et al., 2008) have demonstrated that the predictor expressions for diaphragm flexibility may need to be re-evaluated. Moreover, related studies have demonstrated that the diaphragm in-plane flexibility may lengthen the building period compared to structures with rigid diaphragms (Tremblay, 2005). Given that this building response will affect seismic design, a better understanding of the in-plane shear behaviour of flexible diaphragms is sought.

The scope of this paper is to re-evaluate the diaphragm flexibility expressions of low-rise steel buildings. In this sense, the experimental results of a research investigation conducted on the inelastic behaviour of diaphragms (Essa et al., 2003) as well as the fasteners for steel roof deck diaphragms (Rogers and Tremblay, 2003) are used. Thereafter, numerical models that predict with fidelity the experimental results are prepared. Also, three dimensional nonlinear finite element analyses are performed in order to improve the current code formulas for steel diaphragm design.

2. BACKGROUND RESEACH

Over the past three decades the in-plane shear flexibility, F=1/G', of diaphragms has typically been assessed according to either the SDI (Luttrell, 2004) or ECCS (1977) methods. Both the American and European methods are semi-empirical in nature and are based on the same hypotheses for the

calculation of the total shear flexibility, F, of the diaphragm. The value of F is obtained from a simple summation of individual components of various independent parameters. The resulting flexibility is expressed as follow:

$$F = F_s + F_d + F_c + F_m \tag{2.1}$$

Where F_s is due to the shear deformation of a flat sheet, F_d is due to the warping or distortion deformation of a corrugated profile, F_c is due to the deformation in the sheet at frame and seam fastener locations, and F_m is a miscellaneous flexibility to account either for the axial deformation in the edge members or the deformation between purlins and rafters.
Both methods show some common similarity in the definition of F_s and F_c. However, the flexibility F_d due to the warping deformation is defined differently for each approach. The ECCS method usually results in greater warping flexibility compared with the SDI method. In the SDI method, unlike the ECCS method, the miscellaneous flexibility is neglected and in-plane torsion of the sheets is assumed to not take place. Note; accounting for the miscellaneous flexibility will significantly increase the total shear flexibility of the diaphragm.
A third design approach, known as the Tri-Services method, is also available for use in North America (CSSBI, 2006). This empirical design approach is valid only for a limited number of connector types; including button punch or seam weld side-laps connections and arc spot weld deck-to-frame connections. The total shear flexibility F is defined (Army, 1973) as follows:

$$F = F_1 + F_2 + F_3 \tag{2.2}$$

Where: F_1 is theoretical shear deformation of the diaphragm acting as a flat plate, F_3 describes the flexibility due to the sheet distortion and fastener deformation, F_2 depicts the change in flexibility with regards to the number of spans for single deck. In this approach, it is clearly noticed that there is an interaction between warping deformation and fasteners deformation.

Diaphragm flexibility can also be measured by test as illustrated in Fig. 1. The experimental as well as the numerical shear flexibility, F=1/G', is defined as the reciprocal of the secant stiffness of the shear flow-shear angle curve corresponding to 40% of ultimate strength according to the SDI method.

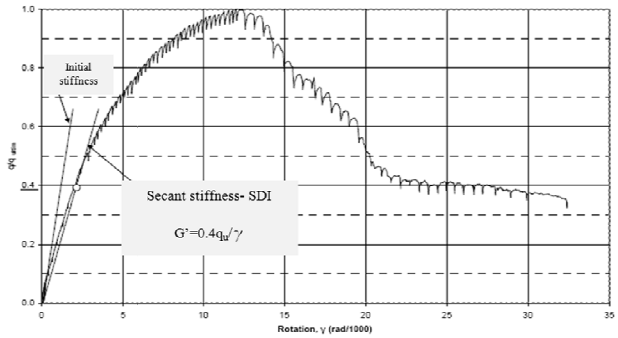

Figure 1. Typical diaphragm response under monotonic shear load (Essa et al., 2003)

3. STEEL DIAPHRAMS STUDIED

As shown in Fig. 2b, large-scale testing of cold-formed steel deck diaphragms with dimension of 6.10 m x 3.66 m was conducted by Essa et al. (2003) to study the inelastic behaviour under monotonic and quasi-static reversed cyclic shear loading. A cantilever diaphragm setup was used, with the load applied parallel to the direction of the deck panels (Fig. 2a). Canam profiled P3606 panels with intermediate ribs having a 38 mm depth, 914 mm width and 6.25 m length were adopted. These profiles are widely used for steel roof deck diaphragms in single-storey buildings in North America.

The cross-section of the profiled panel is shown in Fig. 2c, for which two steel thicknesses were used for test specimens: 0.76 mm and 0.91 mm. Each diaphragm specimen comprised four panels which were supported on equally spaced five purlins (joists). The entire frame was made of rectangular hollow section HSS 203.2 x 203.2 x 7.96 and all connections (purlin-frame) were perfect pins.

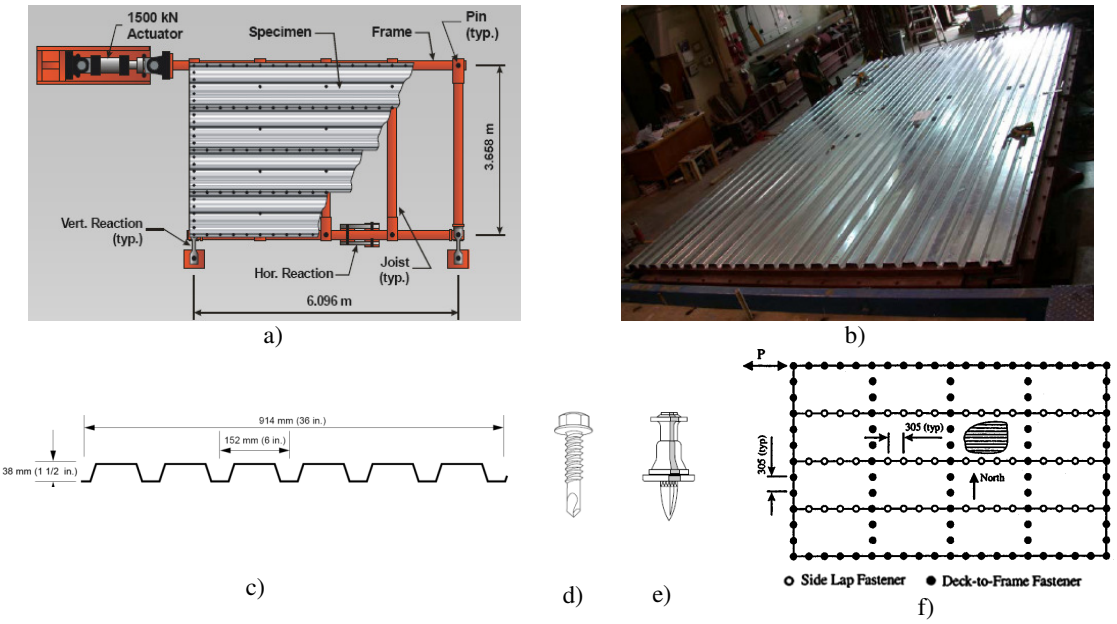

Figure 2. Steel diaphragm test (Essa et al., 2003): a) cantilever diaphragm test setup, b) plan view of tested diaphragm, c) Canam deck profile (nestable), d) Screw fastener, e) Nail fastener, f) Fastener locations

Three different combinations of frame fasteners (deck-to-frame) and side lap fasteners (deck-to-deck) were adopted for the analyses described herein. Screws 10-14x7/8 (Fig. 2d) with 4.8 mm nominal diameter were used to fasten the side laps. Power-actuated fasteners X-EDNK22-THQ12 (Hilti) (Fig. 2e) and BX12 (Buildex) with 5.3 mm nominal diameter were used to connect the deck to the underlying framing. The connector locations for a typical configuration are shown in Fig. 2f; a side lap spacing of 305 mm was used along with a 914/4 frame fastener pattern (fastener every 2nd flute). A selection of three diaphragm configurations, from those tested monotonically by Essa et al. (2003), was used for the purposes of this study (Table 3.1).

Table 3.1. Characteristics of studied diaphragms

Panel no.	Essa test no.	Deck	Deck-to-frame fasteners	Side lap fasteners
DIA1	4	0.76 mm	Nail (Hilti) (914/4)	Screw (305 mm o/c)
DIA2	5	0.76 mm	Nail (Buildex) (914/4)	Screw (305 mm o/c)
DIA3	17	0.91 mm	Nail (Hilti) (914/4)	Screw (305 mm o/c)

4. NUMERICAL MODELLING

4.1. Nonlinear Finite Element Analysis

3D nonlinear analyses were performed using the Abaqus software (standard solver) Version 6.11 (2012) to simulate the large-scale diaphragm tests by Essa et al. (2003) (Fig. 3a). Material nonlinearity and geometric linearity for small displacement were considered. The steel deck panels were discretized using the four node shell elements (S4) having five degrees of freedom per node and five integration points, using Simpson's rule, along the thickness. The frame members and purlins, which supported the panels, were modelled using shell element (S4). A contact property between the frame

elements and the corrugated panels was implemented in order to reproduce realistic boundary conditions (Fig 3b). The frame fasteners were modelled using zero length connectors divided between two discrete points, with six degrees of freedom, two translational nonlinear springs in the plane of the deck, one transitional rigid spring out of the plane of the deck and three rotational rigid springs. The latter was defined in the local axis. The side lap fasteners were modelled using only unidirectional nonlinear springs in the direction of the panels. Fig. 3a illustrates the 6.10 m x 3.66 m diaphragm model used to undertake a parametric study with respect to deck profile, fastener type and fastener pattern. The displacement control loading method was used in the analyses. The Newton-Raphson method was adopted to solve the non-linear equilibrium equations.

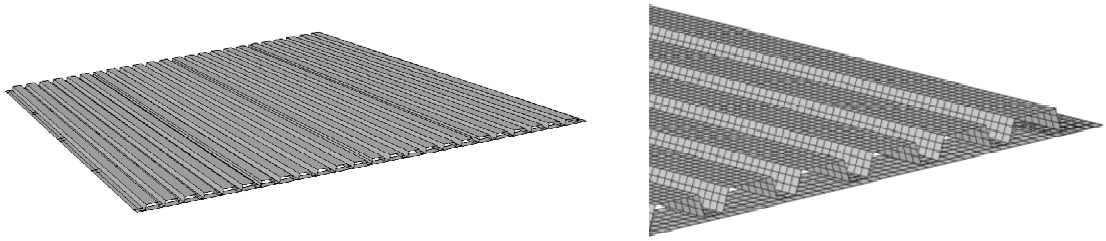

a) b)

Figure 3. FE diaphragm model: a) 3D view of the finite element model, b) Close-up of the finite element mesh.

4.2. Material modelling

ASTM A653 Grade 230 steel having the mechanical properties listed in Table 4.1 was used for the deck panels. Coupon tests on this material carried out by Rogers and Tremblay (2003) were used in the calibration of the FE models. A monotonic tension calibration was performed up to 40% of the strain elongation (Fig. 4) to validate the FE material model.

Table 4.1. Material properties

Deck thickness (mm)	Material property F_y (MPa)	F_u (MPa)	E (GPa)	% elongation
0.76	321	366	208	33
0.91	338	378	197	38

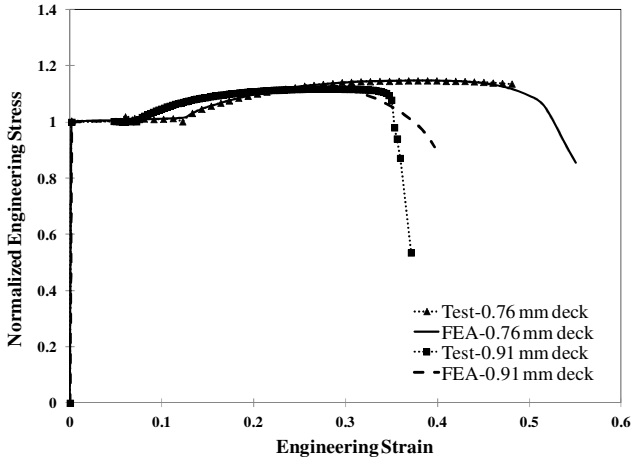

Figure 4. Monotonic tension tests of 0.76 and 0.91 mm coupons compared with FE simulation

4.3. Fastener shear calibration

Each fastener was modelled as a nonlinear spring having the same properties in all directions in the plane of the panel. Although the behaviour of the connection is more complicated than what was modeled (Fig. 5b & Fig 7b), considering the possibility of local fracture and the onset of bearing failure before reaching the ultimate strength of the connected steel sheets, an approach was taken in which the simulation process replicated the global behaviour of the connection including the sheet elements. From this, the nonlinear spring property of a single fastener, including the deck in the connector vicinity, was extracted from the global response, and used in the overall diaphragm model.

4.3.1. Frame fasteners

The calibration of frame fastener behaviour was achieved using data from tests by Rogers and Tremblay (2003a) (Fig. 5a). Connections were composed of a 250 mm long C-shape section (0.76 mm or 0.91 mm thick) joined to a 200 mm long steel plate (3 mm thick plate). Both the Hilti and Buildex nails were used in the scope of testing and for this FE model (Fig. 5b) calibration.

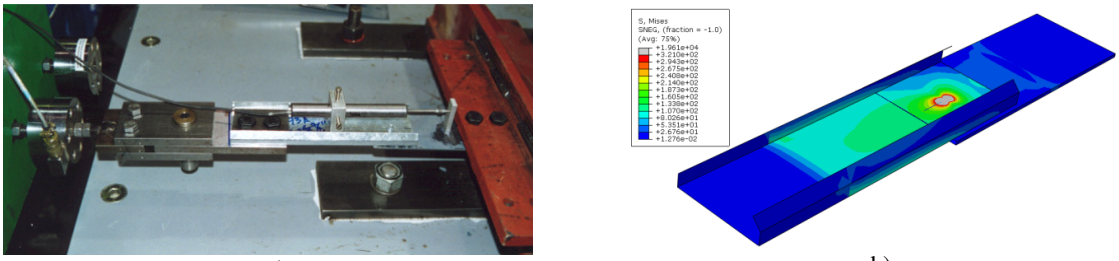

a) b)

Figure 5. Nailed frame fasteners calibration: a) Test setup (Rogers and Tremblay, 2003a), b) FE model.

Comparison of the nonlinear FE model results with the measured connection resistance vs. displacement response is shown in Figure 6. The slope of the first line segment fitted well with the mean monotonic curve, representing three replicate tests (Fig. 6a-c). The slope follows the initial elastic stiffness of the test (K_f-test), and it is close to that determined using the SDI method (K_f-SDI) as described in Table 4.2. The elastic stiffness depends only on the thin plate thickness according to the formulas developed by the SDI approach.

Table 4.2. Deck-to-frame fastener properties

Deck-to-frame connections	Test		SDI		ECCS	
	Stiffness (kN/mm)	Strength (kN)	Stiffness (kN/mm)	Strength (kN)	Stiffness (kN/mm)	Strength (kN)
Hilti (0.76 mm deck)	23.2	6.41	24.1	7.08	40.0	3.70
Buildex (0.76 mm deck)	28.2	6.19	24.1	7.08	40.0	3.70
Hilti (0.91 mm deck)	23.9	7.46	26.5	8.31	-	-

The nonlinear spring property of a single fastener, including the deck in the connector vicinity, was extracted from the response of the entire test specimen (fitted curve of the mean test curve) as shown in Fig. 6d. For each displacement step in the nonlinear analysis, the flexibility of the single fastener was identified as the difference between the flexibilities of the test and an elastic system with a rigid connector. This procedure provided a response from the simulation up to the ultimate strength, which was in good accordance with the mean test curves shown in Fig. 6a-c.

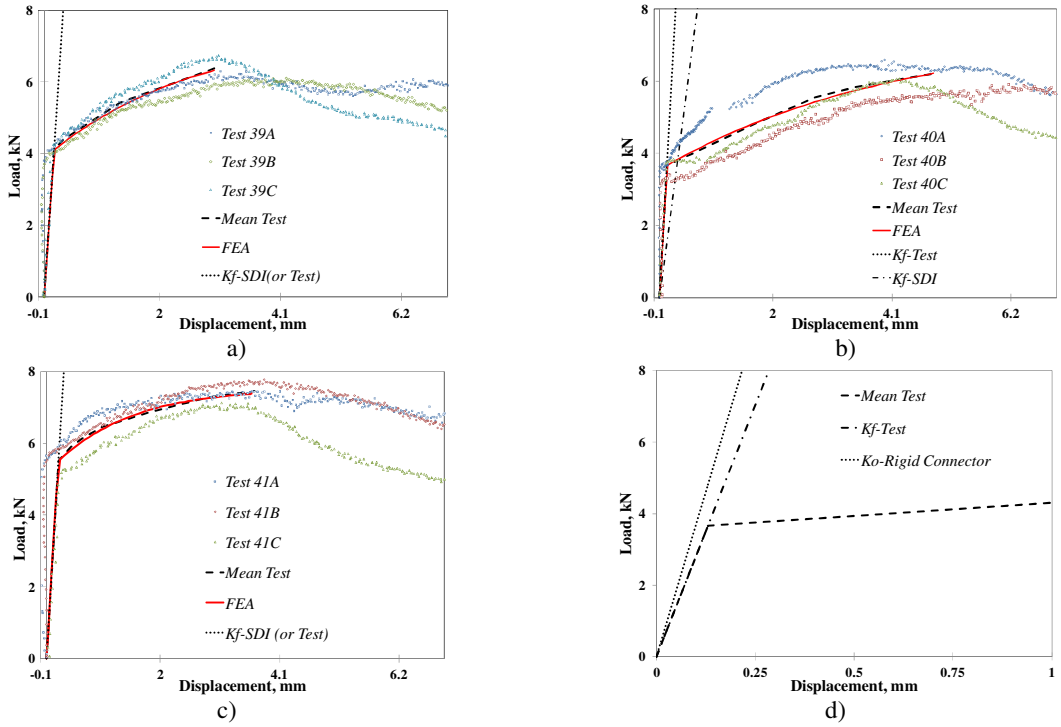

Figure 6. Calibration of frame fastener models: a) Hilti nail in 0.76 mm deck, b) Buildex nail in 0.76 mm deck, c) Hilti nail in 0.91 mm deck, d) Typical calibration curve for frame fastener.

4.3.2. Side lap fasteners

The calibration of side lap fasteners was also carried out using test data from Rogers and Tremblay (2003b) (Fig. 7a) following a similar approach to that implemented for the frame fasteners. The test specimens used for calibration were composed of two adjoining 300 mm long sections of 38 mm deep deck connected with two screws. Figure 7b shows the modelled test specimen under shear loading.

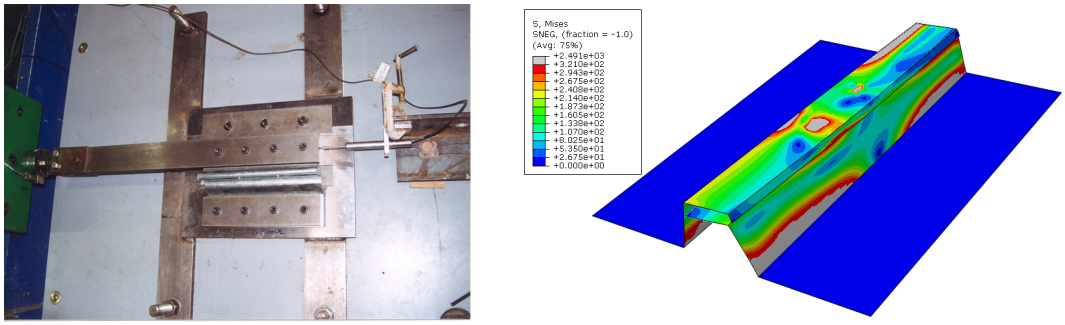

Figure 7. Side lap fastener calibration: a) Test setup (Rogers and Tremblay, 2003b), b) FE model.

Comparison of the nonlinear FE model results with the measured side lap connection resistance vs. displacement response is shown in Figure 8. As found for the frame fasteners, the slope of the first line segment fitted well with the mean monotonic curve representing two replicate tests. This line follows the initial elastic stiffness of the test (K_s-test) and the initial stiffness of a nonlinear system having rigid connectors (Fig. 9). The initial elastic stiffness of the test was completely different from that assessed using the SDI method (K_s-SDI) (Table 4.3), likely due to a difference in the test setup used for development of the SDI equation; however, it was close to that calculated by the ECCS method. It should be noted that that initial tangent stiffness of the analysis results, with or without flexible fasteners, was the same. Based on this evidence, pre-stress and friction properties were created

between the interfaces of the two sheets in the side lap connection model. The value of the in-plane pre-existing force is determined using Fig. 9, corresponds to the point of change of the slope. This procedure allowed for a simulated FE response of the side lap connection that was in good accordance with the mean test curve up to the ultimate strength level (Fig. 8a-b).

Table 4.3. Side lap fastener properties

Side Lap connections	Test		SDI		ECCS	
	Stiffness (kN/mm)	Strength (kN)	Stiffness (kN/mm)	Strength (kN)	Stiffness (kN/mm)	Strength (kN)
Screw (0.76 mm deck)	1.35	2.37	10.0	3.19	1.35	-
Screw (0.91 mm deck)	2.26	3.06	11.1	3.90	1.89	-

As shown in Fig. 9, the nonlinear spring property of the two fasteners, including the deck in the vicinity of the connectors, was extracted from the response of the tested connection (fitted curve of the mean test curve) and the numerical simulation of same specimen with rigid connectors (System1). For this latter model, as evidenced from the nonlinear analysis, the top flange of the deck remained in the elastic domain while the webs of the deck typically became distorted and reached the yield stress.

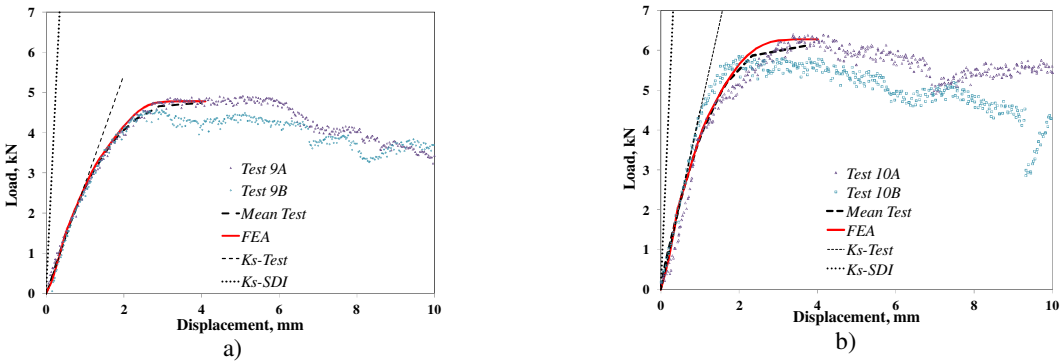

Figure 8. Screw side lap fastener numerical calibration: a) 0.76 mm deck, b) 0.91 mm deck.

For each displacement step in the nonlinear analysis, the flexibility of the two fasteners is the difference between the flexibilities of the test and "System1" with a rigid connector (Fig. 9). This procedure allowed for a response from the simulation up to the ultimate strength of the connection which is in good accordance with the mean test curve (Fig. 8a-b).

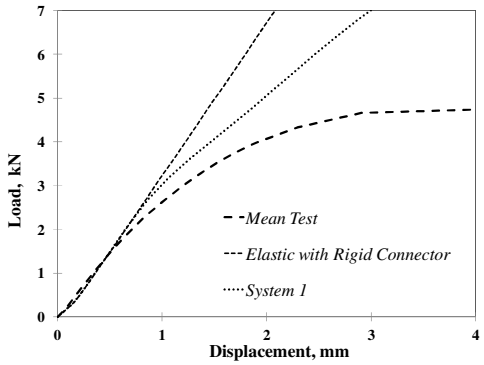

Figure 9. Typical calibration curve for side laps fastener

4.4. Numerical results of diaphragm models

The results obtained from the FE numerical simulation of the diaphragm tests by Essa et al. (2003) are in good agreement with the test results, as shown in Fig. 10. The numerical model was used for the prediction of in-plane shear stiffness of the diaphragm assembly, which was defined as the slope corresponding to 40% of the ultimate strength from the shear flow-shear angle curve according to the SDI method. The shear stiffness predicted using the numerical simulation is compared with the experimental diaphragm results and the formulas of the SDI and ECCS methods in Table 4.4.

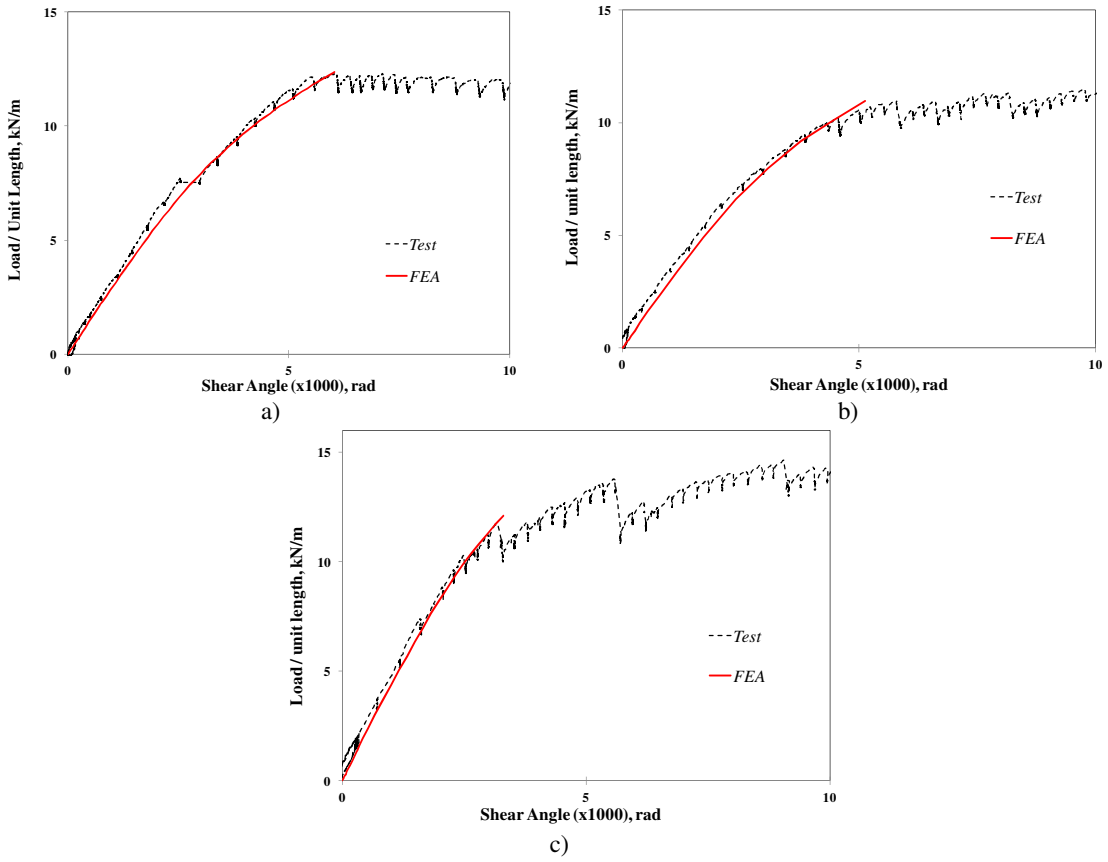

Figure 10. Comparison of load vs. shear angle curves for diaphragm specimens by Essa et al. (2003) vs. numerical simulation: a) DIA1, b) DIA2, c) DIA3.

Figure 11 illustrates the deformed shape of the corrugated panels obtained with the numerical model and that observed during testing. The similarity of the warped profile is noted; this along with the load vs. shear angle graphs in Fig. 10 and the test vs. numerical secant stiffness ratios in Table 4.4 demonstrates the fidelity of the nonlinear finite element model.

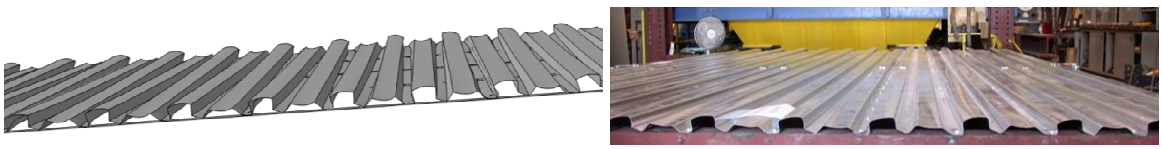

a) b)

Figure 11. Deformed shape of steel deck diaphragm under shear load: a) FE model, b) Test (Essa et al., 2001).

Table 4.4. Measured and predicted shear stiffness values for monotonically loaded diaphragms

		Test shear stiffness (kN/mm)		Numerical vs. Test		Numerical secant vs. Code	
Panel no.	Test load (kN/m)	Initial tang.**	Secant at 40% P_{ult}	Initial tang. ** stif.* ratio	Secant stif.* ratio	SDI stif.* ratio	ECCS stif.* ratio
DIA1	12.3	3.782	3.123	0.827	0.911	0.877	1.434
DIA2	11.5	3.968	3.017	0.795	0.963	0.867	1.432
DIA2	14.6	4.442	4.220	1.086	1.027	0.982	1.511

* Stiffness ** Tangent

The in-plane shear stiffness as predicted with the numerical model is 10% lower than that calculated by the SDI method, which was taken as an indication of the existence of an interaction between the various modes involved in steel deck diaphragm shear deformations. However, the in-plane shear stiffness calculated with the ECCS method is 30% lower than the value predicted numerically. This is due mainly to the warping deformation which is assumed to contribute significantly to the total shear deformation of the roof diaphragm, and is also affected by the miscellaneous flexibility and interaction between the various deformation modes. Note that the warping deformations do provide an important contribution to the total shear deformation, however these deformations which arise from the transverse and out-of-plane displacement of flutes, may be overestimated for 38 mm deep deck panels in the ECCS method. The SDI methodology was developed based on the assumption of transverse displacement but neglected the out-off plane displacement of the deck panel, which in this case resulted in a more accurate prediction of the diaphragm shear stiffness.

Figure 12 describes the three dimensional movement of the deck at a corner of one of the diaphragm specimens tested by Essa et al. (2003). The comparison of the numerical and the experimental measurements at the top of flute provided additional information as to the ability of the numerical model to predict the warping deformation of the deck. As shown in Fig. 13, the predicted shear, u_1, and out-of-plane displacement, u_3, up to 40% of the ultimate strength are similar to the test results. However, the transverse displacement, u_2, was overestimated with the FE model. Further study is required.

a) b)

Figure 12. Deck distortion measurements: a) LVDT Setup (Essa et al., 2001), b) Measurement schematic

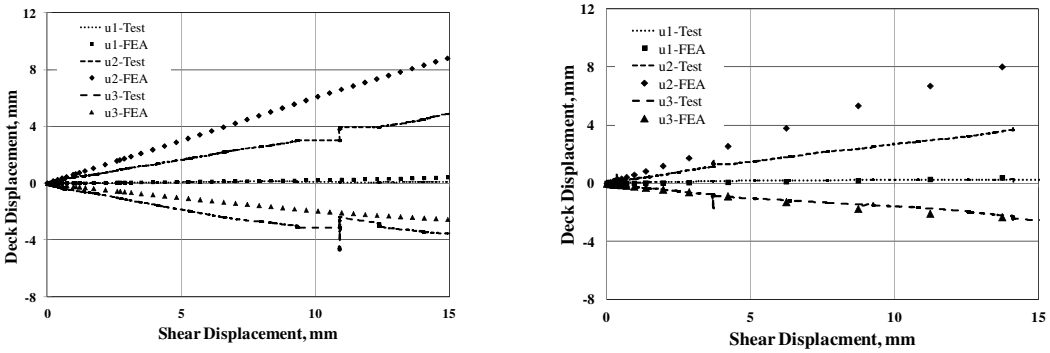

a) b)

Figure 13. Test vs. Numerical simulation deck deformation: a) DIA1, b) DIA2

5. SUMMARY AND CONCLUSIONS

Conclusions are summarized as follows:

1. The numerical simulations show that the Abaqus based nonlinear finite element model proposed in this study can result in predictions of the in-plane shear stiffness of steel deck diaphragms, G', that are in general agreement with test results.
2. This model can be used for the prediction of the in-plane shear behaviour of steel deck diaphragms to investigate the influence of the key parameters such as the fastener pattern, the fasteners type or the deck profile.
3. In-plane shear stiffness as predicted with the numerical model is 10% lower than that calculated by the SDI method.
4. In-plane shear stiffness as predicted with the numerical model is 46% higher than the values calculated with the ECCS method; further study is ongoing to clarify this issue.
5. Compared to the SDI method, the ECCS method appears to give more flexible diaphragms as a result of greater warping flexibility; the flexibility factors $F_{d(\mathbf{ECCS})}$ being more than 20% larger than the corresponding SDI warping flexibility factor $F_{d(\mathbf{SDI})}$.
6. The study indicated that interactions likely exist between the various modes involved in steel deck diaphragm shear deformations, as mentioned in background research; future studies are needed to investigate further this aspect.

AKCNOWLEDGEMENT

Funding for this research was provided by the Natural Sciences and Engineering Research Council of Canada, the Vancouver Steel Deck Diaphragm Design Committee (VSDDC) and its many member companies, the Canadian Sheet Steel Building Institute, the Steel Deck Institute and Hilti Canada.

REFERENCES

Army, U. (1973). Seismic design for buildings *(*No. TM 5-809-10). Washington: Army Navy Air Force.

CSSBI. (2006). Design of Steel Deck Diaphragms, *B13*. Cambridge, Ont., Canada: Canadian Sheet Steel Building Institute.

Dassault Systems Simulia, Corp. (2012). ABAQUS User's Manual, Version 6.11. Providence, RI, USA.

Davies, J. M. (2006). Developments in stressed skin design. *Thin-Walled Structures* **44:12**, 1250-1260.

ECCS. (1977). European Recommendations for the Stressed Skin Design of Steel Structures. European Convention for Constructional Steelwork. ECCS-XVII-77-1E.

Essa, H. S., Tremblay, R., and Rogers, C. A. (2003). Behavior of Roof Deck Diaphragms under Quasi-static Cyclic Loading. *Journal of Structural Engineering*. **129:12**, 1658-1666.

Lamarche, C.-P., Proulx, J., Paultre P., Turek M.,, & Ventura, C. E., Le, T.P., and Levesque C. (2009). Toward a better understanding of the dynamic characteristics of single-storey braced steel frame buildings in Canada. *Canadian Journal of Civil Engineering.* **36:6**, 969-979.

Luttrell, L. D., & Ellifritt, D. S. (1970). Behavior of wide, narrow, and intermediate rib roof deck diaphragms - Preliminary Rep. - phase II. W.Va.: West Virginia Univ.

Lutrell, L. D. (2004). Diaphragm design manual (3rd ed.). Fox River Grove, IL: Steel Deck Institute.

Nilson, A. (1960). Shear Diaphragms of Light Gage Steel. *J. Struct. Div. ASCE* **86:11**, 111-139.

Proulx, J., Boulanger, B., Bakhti, F., Shrestha, K., Tremblay, R., Rogers, C.A., Lamarche, C.P., Paultre, P., (2012). Field measurements and numerical predictions of the dynamic properties of a low-rise steel building with a flexible steel roof deck diaphragm. *Paper presented at the 7th Conference on the behaviour of steel structures in seismic areas STESSA12.*

Rogers, C. A., and Tremblay, R. (2003a). Inelastic seismic response of frame fasteners for steel roof deck diaphragms. Journal of Structural Engineering. **129:12**, 1647-1657.

Rogers, C. A., and Tremblay, R. (2003b). Inelastic seismic response of side lap fasteners for steel roof deck diaphragms. Journal of Structural Engineering. **129:12**, 1637-1646.

Tremblay, R. (2005). Fundamental Periods of Vibration of Braced Steel Frames for Seismic Design. *Earthquake Spectra*. **21:3**, 833-860.

Tremblay, R., Rogers, C. A., Nedisan, C., Franquet, J., Massarelli, R., & Shrestha, K. (2008). Dynamic seismic testing of large size steel deck diaphragms for low-rise building applications. *Paper presented at the 14th World Conference on Earthquake Engineering*.